Journal of Electroanalytical Chemistry 780 (2016) 379–385

Contents lists available at ScienceDirect

Journal of Electroanalytical Chemistry

journal homepage: www.elsevier.com/locate/jelechem

Near-surface solution pH measurements during the pitting corrosion of AISI 1020 steel using a ring-shaped sensor

Marina Medina da Silva, Lucia Helena Mascaro, Ernesto Chaves Pereira, Alexsandro Mendes Zimer *

Laboratório Interdisciplinar de Eletroquímica e Cerâmica (LIEC), Federal University of São Carlos (UFSCar), Chemistry Dept., PO Box: 676, CEP: 13.565-905, São Carlos, SP, Brazil

ARTICLE INFO

Article history:
Received 16 July 2015
Received in revised form 29 January 2016
Accepted 9 February 2016
Available online 13 February 2016

Keywords:
Near-surface solution pH
Ring-shaped pH sensor
Iridium oxide
Pitting corrosion
AISI 1020 steel
In situ optical microscopy

ABSTRACT

This work presents the development and characterization of a ring-shaped sensor built around a steel sample (AISI 1020) to determine the near-surface solution pH (NSSpH) during pitting corrosion. The pH sensor is constituted by a ring of IrO_x, a material that is sensitive to pH changes, synthesized using the Pechini method on a glass tube with a gap of 1 mm between the pH sensor (ring) and the metal sample (disc). The evolution of the corrosion process was also followed using a temporal series of micrographs with an optical microscope. At the same time, the sensor followed the NSSpH during the passivation of the metal, during the breakdown of the passive film, and during the pit evolution in an aqueous basic solution containing HCO_3^- and Cl^- species. When the pit potential was reached, the NSSpH was reduced by one pH unit.

1. Introduction

Several electrochemical processes are strongly influenced by the bulk solution pH and, even more, by changes in its value close to the surface [1–4]. Among such processes, it is well described that corrosion develops in metal/film/solution interfaces and that it is strongly affected by the near-surface solution pH (NSSpH). Considering the Pourbaix diagram for the ternary system iron–sulfide–H_2O [5], the formation of an iron sulfide film only over the pearlitic grains of carbon steel is an experimental result that is not expected [1]. This is an example that can be explained by changes in the NSSpH, which can be rather different from the changes in the bulk. The cementite from the pearlitic grains is a phase of low hydrogen overvoltage and, therefore, it acts as a cathode with respect to ferrite [6]. Because of this, even in an acid solution this phase can present higher pH values than other phases. As the solubility of the sulfide solid decreases with increasing pH, in this case [1], the precipitation of FeS film occurs only over the cementite phase, as observed before in the literature [1,6].

Concerning pitting corrosion, changes in the electrolyte composition in the cavity could stabilize the local galvanic cell action by elimination of the passive state keeping the bottom of the pit in active dissolution. Pickering [7] has showed that different solution compositions which develop inside the pit cavity can influence the magnitude of the potential drop needed to shift its value into the active region. In this sense, Suter et al. [8] used a finite element difference model to simulate the change in the concentration of aggressive species contained in the stagnant solution within the pit cavity. The authors proposed that a stable pit growth occurs when a pit has at least 3 μm of depth, a chloride concentration ($[Cl^-]$) of 6 mol L^{-1}, and a pH of 2 inside the cavity [8]. In another example, the existence of stable pits during the pitting corrosion in dissolved CO_2 environment [9] can be attributed to $FeCO_3$ (siderite) formation, which precipitates inside the pits and induces the acidification of the stagnant solution within the pits. Consequently, the $[Cl^-]$ increases in the pit boundaries to counterbalance the H^+ produced during the formation of siderite film. As consequence of this stabilization, the pits grow on the metal surface. Amri et al. [10] studied the effect of acetic acid on pit initiation and growth in carbon steel immersed in a solution saturated with CO_2. In that paper, it is reported that the pre-initiated pits do not start growing without the presence of this organic acid. These results are strong evidence that the pit depth alone is not enough to keep the bottom of the pit in active dissolution rate. Reactions inside the cavities can produce aggressive species that act on the passive film over the unpitted surface and weaken this protective layer. In other words, the anolyte released from the pits could change the NSSpH, increasing the local generation rate of pits in an autocatalytic effect. Therefore, changes in interfacial pH are directly related to the processes of nucleation, growth, passivation and stabilization of a localized attack on a metal surface.

As described above, changes in the pH value near the interface metal/film/solution are important to the initiation and evolution of the pitting corrosion. To detect such pH changes that, in many cases, do not lead to pH changes in the bulk of the solution, a common glass electrode is inadequate. In this sense, it is necessary to use a different

* Corresponding author.
E-mail address: amzimer@gmail.com (A.M. Zimer).

http://dx.doi.org/10.1016/j.jelechem.2016.02.017
1572-6657/

approach to perform the study. Iridium oxide devices, synthesized using a sol–gel route, could be developed to measure the pH of the solution [11,12]. Iridium oxide is a promising material due to its stability and sensitivity; besides, such synthesis method allows the miniaturization of the pH device in a needle configuration [11], for example, or any other complex shape that the experimentalist wants. In this sense, in a previous work [12], we developed a rotating ring/disc electrode which was an ultramicroelectrode for pH measurements that could be applied under hydrodynamic control or to measure the NSSpH when such setup was used in stationary mode. The disc electrode can be built of any material to investigate the NSSpH in many systems. In the present work, we have explored the application of such device in stationary mode to detect pH changes close to the interface during the pitting corrosion of AISI 1020 steel in aqueous basic solution, containing HCO_3^- and Cl^- species, coupled to both, an electrochemical technique and an in situ optical microscopy measurement.

2. Experimental

2.1. Construction of pH ring-shaped sensor on a ring-disc electrode

This pH sensor was built following a previously described procedure [13]. In the present case, the disc material used was an AISI 1020 steel rod inserted into the glass tube, Fig. 1a. A polymeric precursor made of citric acid (CA), ethylene glycol (EG), and $IrCl_3$ (Ir) in a molar ratio of 0.5:3:12 (Ir:AC:EG) was painted on the glass tube. Then, the system was submitted to a calcination step at 400 °C for 10 min and, as consequence, IrO_x was formed on the substrate, Fig. 1a. The process was repeated four times to increase the thickness of the oxide layer [13]. Then, electrical contacts were made and the device was sealed with Araldite® and epoxy resin that formed the body of the ring-disc electrode, Fig. 1a. Fig. 1b shows a photo of the final electrode where the ring (sensor) and the disc (steel sample) can be better observed. The glass tube has an inner and outer diameter of 5 mm and 7 mm, respectively. The gap between the sensor and the metal sample is of 1 mm and the IrO_x ring over the tube has a thickness of 6.5 ± 2.0 μm, see insets of Fig. 1b.

The ring-disc configuration has been used before in the literature to pH measurements by Albery and Calvo with a bismuth ring [14,15] and by Steegstra and Ahlberg [16] with a platinum disc, both in a commercial ring-disc electrode, where a metal oxide was chemical or electrochemical deposited to be as a pH sensor. However, the ring-shaped sensor described in Fig. 1 has some advantages, for instance, polishing of the disc electrode does not destroy the pH sensor, on the contrary, renews it. This is possible due to the special shape of the IrO_x deposit. As observed in Fig. 1a the ring is a tube of oxide that can be abraded or polished keeping the horizontal level of the disc and the ring. It is an important advantage in the investigation of an active metal disc material, such as in the present case.

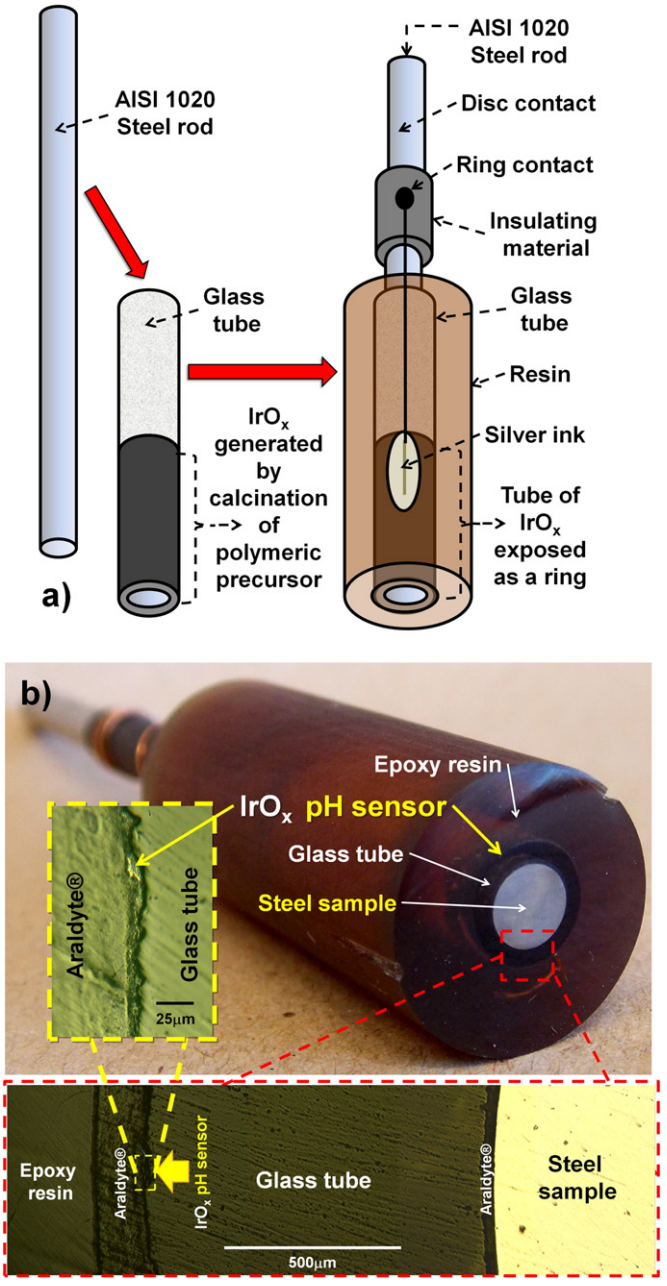

Fig. 1. Flowchart describing the experimental procedure for assembly of IrO_x pH sensor (a). Photo of ring-disc electrode showing from right to left: the steel sample (AISI 1020) as a disc in the center of electrode, glass tube, ring-shaped sensor of IrO_x used as pH sensor, and the epoxy resin (b). Optical micrograph showing the gap between the steel sample and the pH sensor (inset). Zoom of IrO_x pH sensor (inset).

2.2. Carbon steel sample

Cylindrical AISI 1020 steel (Sanchelli) with a diameter of 4.8 mm (A = 0.18 cm^2) was used as disc working electrode (WE) (see Fig. 1b). Their chemical composition was determined by Atomic Absorption Spectroscopy (ASS) analysis: 0.186% C, 0.509% Mn, 0.030% S, 0.003% P, 0.022% Cr, 0.013% Ni, 0.020% Mo, 0.017% Cu, 5×10^{-4}% Al, 0.106% Si, wt.%, and Fe balance. This material was used as received. The metallic surface morphology was observed after an etching process to reveal the grain size and inclusions in the sample. The etching was carried out using a fresh Nital 2% solution following a common procedure described elsewhere [17].

Prior to use, the ring-disc electrode was abraded with sandpaper from 320 up to 1200-grit, polished with alumina (0.3 μm), and then washed with deionized water for 30 s in an ultrasonic bath.

2.3. Equipment and techniques

A pH-meter (Denver, Ultrabasic, mod. UB-10) was used to carry out potentiometric titrations as the calibration system for the IrO_x pH sensor before the corrosion tests. These experiments were performed simultaneously with a combined glass electrode mod. CW711X/Qualxtrom.

An Autolab Potentiostat/Galvanostat (PGSTAT 30) with GPES 4.9.006 software was used to perform the corrosion tests, see PC-1 in Fig. 2. The reference electrode, RE_1, and the counter electrode, CE, were a Ag/AgCl/KCl (sat.) and a circular Pt sheet, respectively.

The IrO_x ring-shaped sensor was used as a potentiometric sensor for pH measurements where the E_{pH} was monitored using a digital multimeter (Minipa ET-2231A) interfaced to a computer, see PC-2 in

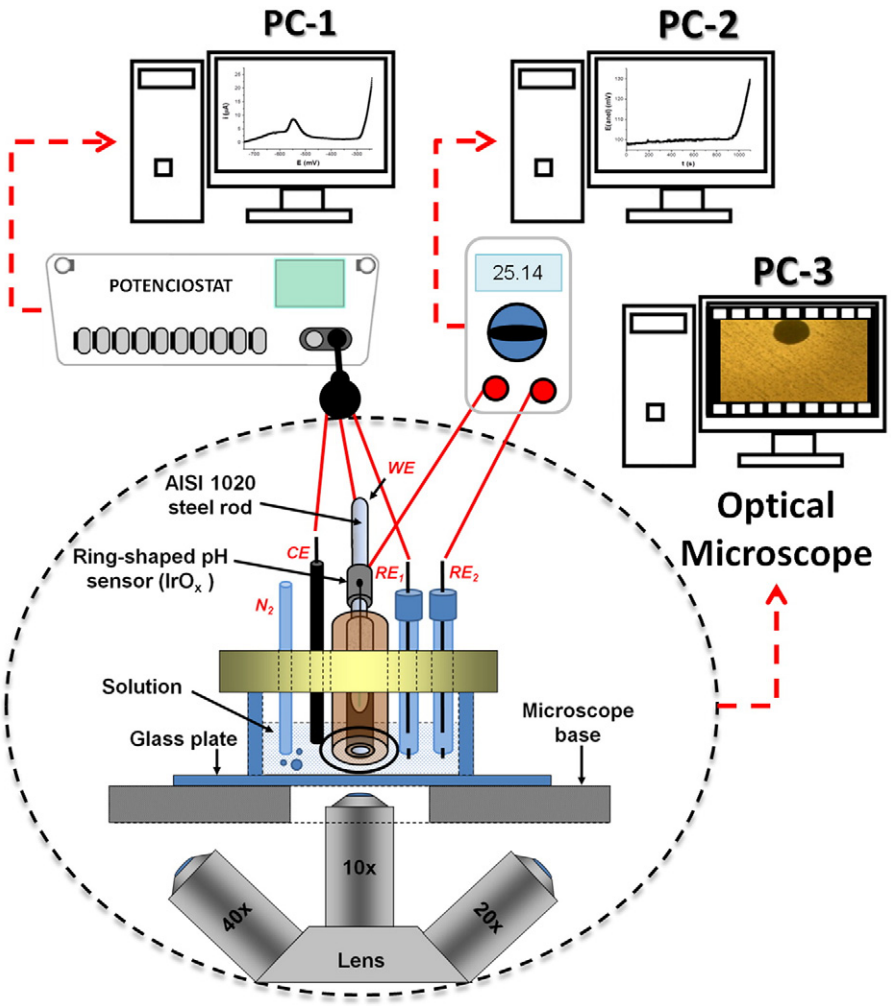

Fig. 2. Schematic diagram describing the connections between the equipment used: potentiostat, multimeter and the optical microscope, respectively. Electrochemical cell with inputs for: CE, RE_1, RE_2, N_2 flux and the WE.

Fig. 2. This potential was measured with respect to another Ag/AgCl/KCl (sat.), RE_2.

The carbon steel disc was observed in situ using an inverted OM (Opton, TNM-07T-PL model) to obtain a temporal series of micrographs, TSM, in a region which corresponds to 8.2% of the WE surface (680 μm × 544 μm), see PC-3 in Fig. 2. This measurement was performed using a flat-bottom cell [1] and the Scope Photo® 1.0 and MCDE (AMCAP) software were used for data acquisition. The same procedure employed in previous papers to follow the pitting corrosion [18] was applied here to analyze the in situ TSM giving as final results: the number of pits and the total pit area. The image acquisition rates used were 0.05 and 1 image s^{-1} during the open circuit potential, E_{oc}, and during the polarization curves, PC.

A schematic diagram is shown in Fig. 2 describing the experimental setup during the simultaneous measurements together with a detailed description of the components on the electrochemical cell.

2.4. Experimental procedure

The calibration of the ring-shaped sensor was made by titration curves of NaOH 0.1 mol dm^{-3} (Quimis) with H_3PO_4 1.0 mol dm^{-3} (Mallinckodt) performed simultaneously with a combined glass electrode.

All solutions were prepared using reverse membrane purified Milli-Q water (Millipore). The pitting corrosion was studied in a deoxygenated 0.1 mol dm^{-3} $NaHCO_3$ solution (Merck). The pH of this solution was 8.3 (bulk pH) due to the buffering action of carbonate species [9,19]. In this solution, NaCl (JT Backer) was added to produce a 3.0 wt.% NaCl solution (0.51 mol dm^{-3} NaCl) to induce adequate conditions for pitting corrosion to occur.

To investigate the passivation of the metal, the E_{oc} was monitored until the steady state was reached while the TSM and the E_{pH} were obtained to follow the corrosion process with the in situ micrographs and the pH data in the near-surface solution, respectively.

The anodic PC was performed at $\nu = 0.5$ mV s^{-1} with $\Delta E = 500$ mV while the TSM and E_{pH} were monitored using the same temporal resolution. The TSM was analyzed using the ImageJ program, following a procedure previously described [1,18,20], to obtain the number of pits and the total pit area in each electrochemical experiment.

3. Results and discussion

3.1. Characterization of the metal surface

The metallographic study of AISI 1020 steel is shown in Fig. 3. The fresh polished surface is shown in Fig. 3a where some scratches, defects, and inclusions can be observed. In agreement with the literature, the inclusions are composed by MnS and they are evenly distributed throughout the alloy as black spots. Fig. 3b shows the same surface after etching using a fresh 2% Nital solution during 10 s of attack [17]. Using the ASTM E 1382-97 [21], the pearlitic phase was determined as 29 ± 4% of the

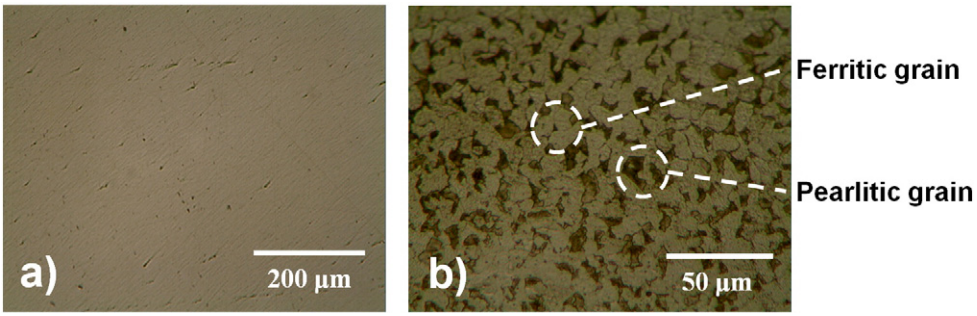

Fig. 3. Metallographic analysis of AISI 1020 steel before (a) and after chemical etching for 10 s in fresh 2% Nital solution (b). Pearlitic and ferritic phases are marked with dotted circles.

surface area, and the average size of pearlitic grains as 3.3 ± 0.6 µm^2 (Fig. 3b).

3.2. Characterization of the ring pH sensor

Fig. 4a shows an acid–base titration of 0.1 mol dm^{-3} NaOH solution through dropwise addition of 1.0 mol dm^{-3} H_3PO_4 solution using the ring-shaped pH sensor here investigated. Simultaneously, a conventional pH glass electrode was used to check the pH sensor quality. As can be observed, the behavior of E_{pH} is very close to the pH determined with conventional pH electrode. The potentiometric response of the ring-shaped sensor of IrO_x, as a function of solution pH, is shown in Fig. 4b. In this figure, a linear response in the 3.5–12 pH range was observed with a slope of 24.9 mV pH^{-1}. This slope was used to convert the E_{pH} into pH changes near the surface.

The low sensitivity of the ring-shaped sensor of IrO_x could be related to the absence of a metal substrate on the metal/metal oxide interface, as presented in Fig. 1a, the iridium oxide was generated by calcinations over a glass substrate, without any conductive substrate. Even this type of sensor being based on equilibrium between different oxidation states [16], we believe that this electrode could also have a contribution from the sensors of the first category, in which the pH dependence would come from the redox equilibrium between the metal and its oxide [16]. In this sense, this hypothesis is outside the scope of the present paper and will be further investigated in a future study. Other hypothesis for the low sensitivity could be attributed to different mechanisms that produce such changes in a microelectrode configuration. In the literature [22] it was observed that the miniaturization of the electrode could change the slope from 58.5 to 80.5 mV pH^{-1} due to the different mechanisms below and above pH 6. We observed such behavior in our configuration below pH 4 but, for the application presented here, such behavior was not showed here. For more details, the slope change below pH 4 was investigated before in the literature in the following reference [13].

To verify if the sensibility of the ring-shaped pH sensor could be affected by solution properties during the corrosion analysis, a titration was performed in the pH range 8.3–6.3 using the same solution from corrosion experiments (0.1 mol dm^{-3} $NaHCO_3$ containing 3.0 wt.% [Cl$^-$]) by addition of 1.0 mol dm^{-3} HCl to this medium. It was observed that, in this range, the pH sensor kept the same sensibility observed in Fig. 4b.

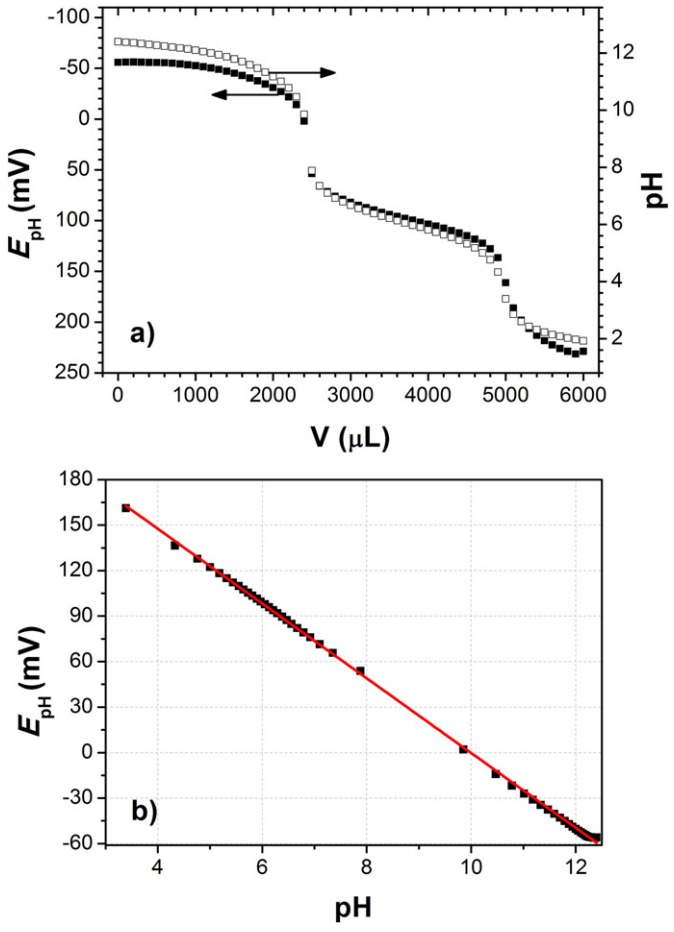

Fig. 4. Titration curve of NaOH (0.1 mol dm^{-3}) titrated with H_3PO_4 (1 mol dm^{-3}) (a). Calibration curve for E_{pH} as a function of the pH (b). Potential of IrO_x pH sensor versus Ag/AgCl/KCl (sat.).

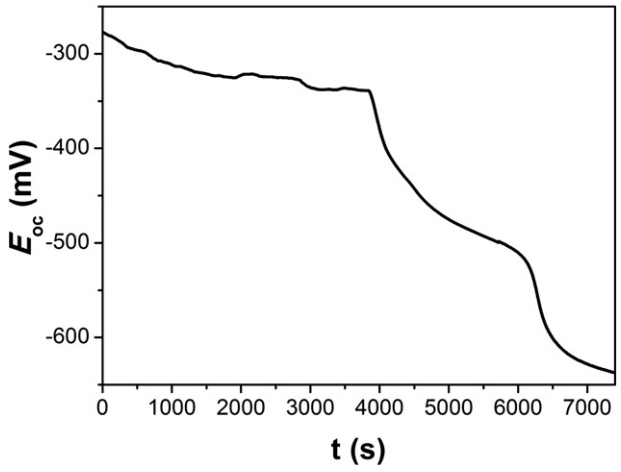

Fig. 5. E_{oc} of AISI 1020 steel in solution of 0.1 mol dm^{-3} $NaHCO_3$ with 3.0% [Cl$^-$]. All potential values versus Ag/AgCl/KCl (sat.).

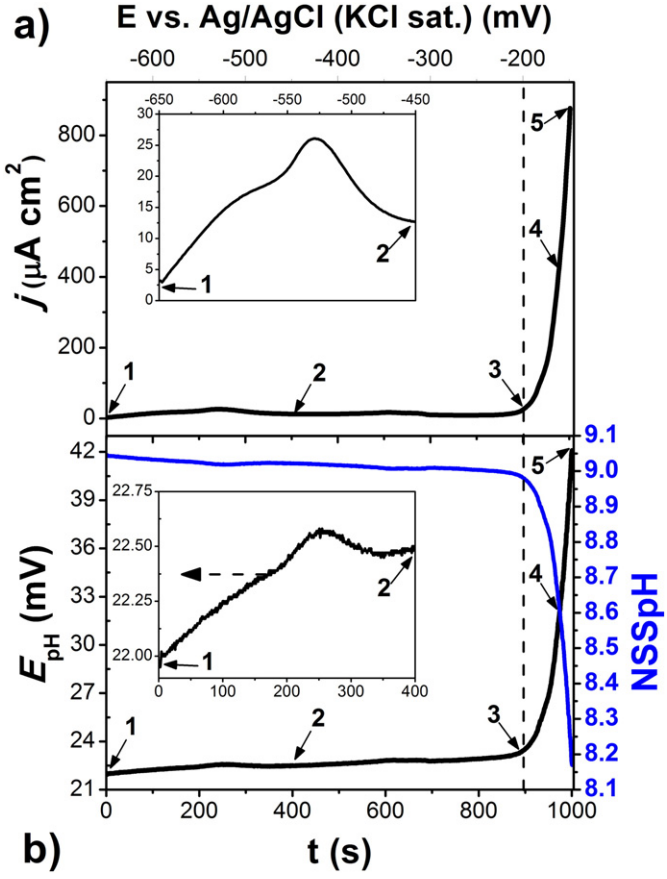

Fig. 6. PC of AISI 1020 steel in solution of 0.1 mol dm^{-3} $NaHCO_3$ with 3.0% [Cl^-] (a), E_{pH} during the PC measured with the ring-shaped sensor (b), and NSSpH based on the slope of 24.9 mV pH^{-1} (Fig. 4b). All potential values versus Ag/AgCl/KCl (sat.).

3.3. PC coupled to near-surface pH measurements

Fig. 5 shows the E_{oc} of AISI 1020 steel in a 0.1 mol dm^{-3} $NaHCO_3$ solution containing 3.0 wt.% [Cl^-] until the disc potential stabilization. The initial region of constant E_{oc} is known as the induction period [23], where the initial stage of pitting corrosion is initiated on the defects and/or inclusions of the carbon steel. A sharp drop to more negative potential values is typical of pitting corrosion process [23]. After this potential drop the steady state was observed, where the passivation process with the formation of $FeCO_3$ film could happen by the following equation, according to the Pourbaix diagram [5,24]:

$$Fe_{(s)} + HCO_3{}^-{}_{(aq)} \rightarrow FeCO_{3(s)} + H^+{}_{(aq)} + 2e^- \quad (1)$$

Reffass et al. [24] present the potential-pH diagrams for iron in aqueous $NaHCO_3$ solution summarizing all thermodynamic information and possible routes in such environment. According to the author, in this pH range the reaction of Eq. (1) is favored on the metal surface.

After the steady state, Fig. 6a shows a PC carried out at a scan rate of 0.5 mV s^{-1}. The scan was started at −0.65 V (E_{oc}) in the anodic direction and, at the same time, the NSSpH was followed through the ring-shaped sensor, Fig. 6b. In this figure, the E_{pH} is shown on the left side of Fig. 6b and, using the calculated slope of 24.9 mV pH^{-1} (Fig. 4b), the NSSpH is shown in the right axis of this figure. Besides the pH measurements, the TSM was recorded. The arrows at the times of 0 (#1), 400 (#2), 900 (#3), 950 (#4), and 1000 s (#5) represent the frames presented in Fig. 7. The regions highlighted in Fig. 7 with dotted squares are amplified to evidence the surface behavior during the experiment.

During the passivation process (magnified region of Fig. 6a), it is possible to observe that the E_{pH} (Fig. 6b) increases slightly and then decreases. This indicates that the NSSpH had an opposite behavior between instants "1" and "2" of Fig. 6b, i.e., a small decrease followed by an increase in the NSSpH was observed. This last increase in the NSSpH after the passivation peak is expected because the passive film formation is favored in such condition, according to the Pourbaix diagram [5,24].

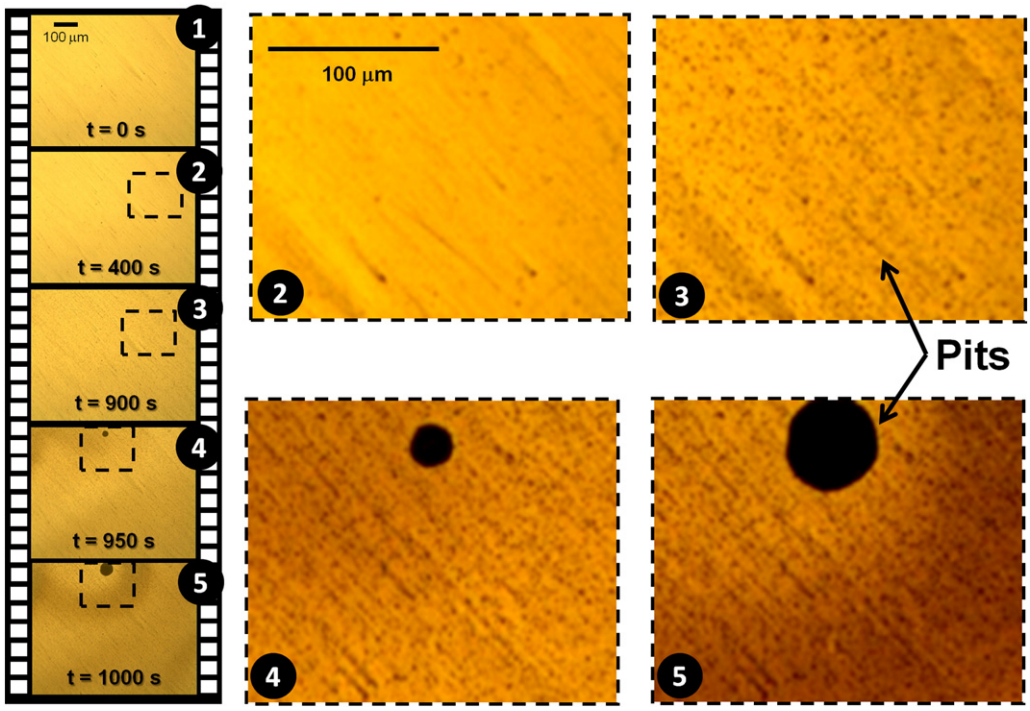

Fig. 7. In situ micrographs from TSM taken at the instants marked as 0 (#1), 400 (#2), 900 (#3), 950 (#4), and 1000 s (#5) in Fig. 6. The regions marked with dotted squares are amplified to evidence the surface behavior during the experiment (insets).

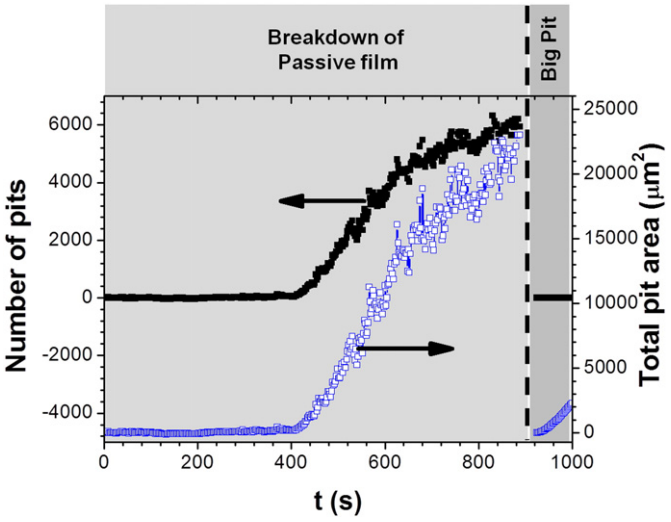

Fig. 8. Analysis of TSM to obtain the number of pits and total pit area as function of the potential applied during the PC of Fig. 6a. Gray regions show the analysis for the pits observed during the breakdown of the passive film and for the big pit observed in Fig. 6b.

From 400 s up to 900 s (Fig. 6b), the NSSpH decreases again, which could be related to the breakdown of the passive film in agreement with Eq. (1) which leads to a continuous formation of H^+ in the electrode/solution interface. Therefore, siderite ($FeCO_3$) could precipitate within the pits (regions where the film collapsed) as soon as the anodic dissolution of the iron begins [9]. This reaction could explain the changes in the NSSpH on the electrode/solution interface, and also, the large number of pits observed in Fig. 7 from 400 to 900 s (instants "2" and "3").

During the sharp increment in current density in Fig. 6a, between instants "3" and "5", it was observed that one big pit had grown on the metal surface (see instants "4" and "5" in Fig. 7). As consequence, a proportional change in the NSSpH was recorded in this region. According to the slope of Fig. 4b this value corresponds to a final pH in the electrode/solution interface of approximately 8.1 at the end of the anodic PC, Fig. 6b. This result shows that a variation of one pH unit occurs in the neighborhood of the surface comparing to its initial value, pH 9.1.

3.3.1. Analysis of TSM

The entire TSM, recorded using the experimental setup described at Fig. 2, was analyzed following a procedure previously described in the literature [1,18,20]. After image treatment the number of pits and the total pit area were calculated during the PC and are presented in Fig. 8. This figure presents data for the pits observed during the breakdown of the passive film, between instants "2" and "3" of Fig. 7, and for the big pit observed between instants "4" and "5" in the same figure.

The main advantage of TSM used together with NSSpH data is that it is possible to estimate when the passive film breakdown occurs, which is, in the present case, near 400 s (Fig. 8) when the nucleation of many pits can be observed [25,26,27]. Sharland [28] has reported that the initiation of pit corrosion requires two main events: i) there must be points of breakdown of the passive film followed by ii) the activation of the metal surface. Marcus et al. [27] highlight that, generally, films are crystalline or get crystalline with the exposition time to the aggressive environment. In this sense, the thinning mechanism of the passive film is also related to the microstructure of the film itself when a high number of nanograins, separated by grain boundaries, exist in the passive layer and could become pit nucleation sites [27]. As the polarization continues, the number of pits grow up to a stabilization at approximately 6000 pits after 740 s. Analyzing the total pit area, also presented in Fig. 8, a change in the slope was observed when the number of pits became constant. Based on the previous work [20], these two distinct growth rates were calculated (Table 1), before and after 740 s, and were named regions A and B, respectively. These pit growth rates highlight two different moments in the passive film breakdown. In region A, the nucleation of pits occurs together with their growth over the metal surface followed by a transition to region B, where the stable pits govern the process [20]. This proposition could explain the reduction of this second growth rate after the number of pits gets constant in region B, Table 1.

Finally, the big pit observed in Fig. 7 had its growth rate calculated in region C in Table 1 (data based on the entire TSM from Fig. 8). This big pit had a growth rate of $36.7 \pm 0.5\ \mu m^2\ s^{-1}$ similar to the growth rate of the stable pits ($32.2 \pm 2.3\ \mu m^2\ s^{-1}$) in region B (Table 1), therefore, within the region where the pit growth is dominant.

A surface mapping, conduced after the last experiment, showed approximately 30 big pits. Therefore, it is possible to propose that the strong variation in the NSSpH observed in Fig. 6b could be due to the anolyte released from the big pits on the metal surface during the anodic polarization experiment.

Table 1
Total pit area changes in Region A (410–740 s) and in Region B (740–890 s) during the PC experiment presented in Fig. 6a.

Exp.	Total pit area changes/$\mu m^2\ s^{-1}$		
	Region A (410–740 s)	Region B (740–890 s)	Region C (940–1000 s)
Fig. 8	59.5 ± 1.3	32.2 ± 2.3	36.7 ± 0.5

4. Conclusions

This work shows the construction of a ring-shaped pH sensor, using the polymeric precursor method (Pechini), to study the pit corrosion of carbon steel in aqueous basic solution containing HCO_3^- and Cl^- species.

The pH response of IrO_x ring was investigated using acid–base titrations and showed a linear behavior within the range $3.5 < pH < 12$ with a slope of 24.9 mV pH^{-1}. The thickness of the IrO_x ring was (6.5 ± 2.0) μm, which characterizes the electrode as an ultramicroelectrode for pH measurements. The ring-disc electrode was used in stationary mode to allow the observation of the metal surface using a coupled optical microscopy measurement.

In the anodic polarization of the carbon steel, the ring-disc electrode was sensible enough to detect pH changes near the electrode surface during the passivation process and during the breakdown of the siderite passive film. A decrease of one pH unit in the NSSpH was observed when the pit potential was reached; at the same time, the in situ TSM showed that big pits were developing in this region during the PC.

Acknowledgments

The authors would like to thank FAPESP (grant #13/13503-0, #11/19430-0, #2013/07296-2), CNPq and CAPES for financial support.

References

[1] A.M. Zimer, E.C. Rios, P.C.D. Mendes, W.N. Gonçalves, O.M. Bruno, E.C. Pereira, L.H. Mascaro, Investigation of AISI 1040 steel corrosion in H2S solution containing chloride ions by digital image processing coupled with electrochemical techniques, Corros. Sci. 53 (2011) 3193–3201.
[2] J.S. Santos, F. Trivinho-Strixino, E.C. Pereira, Investigation of $Co(OH)_2$ formation during cobalt electrodeposition using a chemometric procedure, Surf. Coat. Technol. 205 (2010) 2585–2589.
[3] J.S. Santos, R. Matos, F. Trivinho-Strixino, E.C. Pereira, Effect of temperature on Co electrodeposition in the presence of boric acid, Electrochim. Acta 53 (2007) 644–649.
[4] A. Brenner, Electrodeposition of alloys. Principles and practice, Academic Press, New York, London, 1963.
[5] M. Pourbaix, Atlas of electrochemical equilibria in aqueous solution, second ed. NACE International, Houston, 1974.
[6] H.H. Huang, W.T. Tsai, J.T. Lee, Electrochemical behavior of the simulated heat-affected zone of A516 carbon steel in H2S, Electrochim. Acta 41 (1996) 1191–1199.

[7] H.W. Pickering, The significance of the local electrode potential within pits, crevices and cracks, Corros. Sci. 29 (1989) 325–341.
[8] T. Suter, E.G. Webb, H. Böhni, R.C. Alkire, Pit initiation on stainless steels in 1 M NaCl with and without mechanical stress, J. Electrochem. Soc. 148 (2001) B174–B185.
[9] M. Reffass, R. Sabot, M. Jeannin, C. Berziou, Ph. Refait, Effects of phosphate species on localised corrosion of steel in NaHCO3 + NaCl electrolytes, Electrochim. Acta 54 (2009) 4389–4396.
[10] J. Amri, E. Gulbrandsen, R.P. Nogueira, The effect of acetic acid on the pit propagation in CO_2 corrosion of carbon steel, Electrochem. Commun. 10 (2008) 200–203.
[11] A.M. Zimer, S.G. Lemos, L.A. Pocrifka, L.H. Mascaro, E.C. Pereira, Needle-like IrO_2/Ag combined pH microelectrode, Electrochem. Commun. 12 (2010) 1703–1705.
[12] A. Fog, R.P. Buck, Electronic semiconducting oxides as pH sensor, Sensors Actuators 5 (1984) 137–146.
[13] A.M. Zimer, M.M. da Silva, E.G. Machado, H. Varela, E.C. Pereira, L.H. Mascaro, Development of a versatile rotating ring-disc electrode for in situ pH measurements, Anal. Chim. Acta 897 (2015) 17–23.
[14] W.J. Albery, E.J. Calvo, Ring-disc electrodes part 21. — pH measurement with the ring, J. Chem. Soc. Faraday Trans. 1 79 (1983) 2583–2596.
[15] W.J. Albery, A.R. Mont, Ring-disc electrodes part 23. — studies of proton fluxes at a thionine-coated electrode, J. Chem. Soc. Faraday Trans. 1 85 (1989) 1189–1198.
[16] P. Steegstra, E. Ahlberg, Influence of oxidation state on the pH dependence of hydrous iridium oxide films, Electrochim. Acta 76 (2012) 26–33.
[17] C.B. Frederick, E.S. Daniel, Improved metallographic etching techniques for stainless steel and for stainless steel to carbon steel weldments, Metallography 9 (1976) 91–107.
[18] A.M. Zimer, M.A.S. De-Carra, E.C. Rios, E.C. Pereira, L.H. Mascaro, Initial stages of corrosion pits on AISI 1040 steel in sulfide solution analyzed by temporal series micrographs coupled with electrochemical techniques, Corros. Sci. 76 (2013) 27–34.
[19] P. Atkins, J. De Paula, Physical chemistry (Atkins) — 8th edition, New York, Oxford, 2006.
[20] A.M. Zimer, M.A.S. De-Carra, L.H. Mascaro, E.C. Pereira, Temporal series of micrographs coupled with electrochemical techniques to analyze pitting corrosion of AISI 1040 steel in carbonate and chloride solutions, Electrochim. Acta 124 (2014) 143–149.
[21] Standard Test Methods for Determining Average Grain Size Using Semiautomatic and Automatic Image Analysis, ASTM E 1382-97, NTU, 1997 855–878.
[22] D.O. Wipf, F. Ge, T.W. Spaine, J.E. Baur, Microscopic measurement of pH with iridium oxide microelectrodes, Anal. Chem. 72 (2000) 4921–4927.
[23] A.D. Davydov, Analysis of pitting corrosion rate, Russ. J. Electrochem. 44 (2007) 835–839.
[24] M. Reffass, R. Sabot, C. Savall, M. Jeannin, J. Creus, Ph. Refait, Localised corrosion of carbon steel in $NaHCO_3$/NaCl electrolytes: role of Fe(II)-containing compounds, Corros. Sci. 48 (2006) 709–726.
[25] Z. Szklarska-Smialowska, Pitting corrosion of metals, NACE, Houston, Texas, 1986.
[26] T.P. Hoar, The production and breakdown of the passivity of metals, Corros. Sci. 7 (1967) 341–355.
[27] P. Marcus, V. Maurice, H.-H. Strehblow, Localized corrosion (pitting): a model of passivity breakdown including the role of the oxide layer nanostructure, Corros. Sci. 50 (2008) 2698–2704.
[28] S.M. Sharland, A review of the theoretical modelling of crevice and pitting corrosion, Corros. Sci. 27 (1987) 289–323.